

$H \times W \times T$ ($= 65 \times 10 \times 0.2 \text{ mm}^3$) is illustrated in Figure 1(a). A $50 \text{ } \Omega$ coaxial probe centrally feeds the bottom of the strip through an SMA connector, and the gap between the bottom and the ground plane is $h = 1 \text{ mm}$. Figure 1(b) provides side-view figures of the monopole antenna with the parasitic planar element. The parasitic element is a square copper plate with dimensions of $L \times L \times t$ ($= 48 \times 48 \times 0.2 \text{ mm}^3$). The spacing between the bottom of the square plate and the ground plane is the same as the dimension $h = 1 \text{ mm}$. There is an offset $D = 18 \text{ mm}$ between the axial lines of the square and the strip. The square plate is placed in parallel to the strip face to face at a distance $d = 0.2 \text{ mm}$. We measured the input impedance with an HP8510C network analyzer. In the tests, a $320 \times 300 \text{ mm}^2$ rectangular copper plate was used to approximate the ground plane.

Figure 2 provides the measured input impedance and VSWR of the typical narrow strip monopole antenna shown in Figure 1(a) within the range from 1 to 9 GHz. When the corresponding height normalized by the wavelength H/λ changes from 0.22 to 1.95, it is found from Figure 2 that there are four passbands appearing around 1, 3.2, 5.5, and 7.8 GHz, respectively. Then, we introduced the parasitic square plate electromagnetically coupled to the monopole as shown in Figure 1(b). Its dimensions L normalized by the wavelengths are 0.16 at 1 GHz and 1.44 at 9 GHz, respectively. Due to the proximity of the monopole and the plate, the input impedance changes quite a bit, as shown in Figure 3. A measured VSWR of less than 2 has been realized across the 1.1–8.7 GHz band.

3. CONCLUSION

A monopole antenna with a parasitic planar square element has been proposed. Measurements on the input impedance have been conducted. A 1:8 impedance bandwidth has been

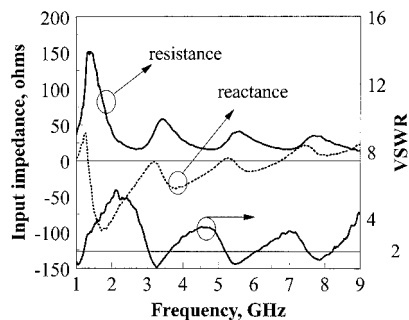


Figure 2 Measured frequency response of the strip monopole antenna, including input impedance and VSWR

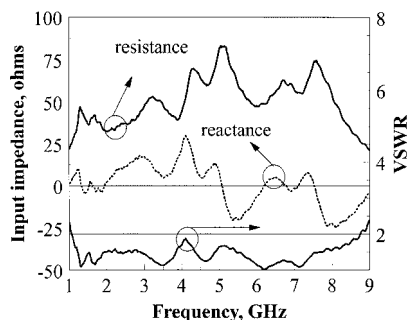


Figure 3 Measured frequency response of the monopole antenna with a parasitic element, including input impedance and VSWR

readily attained with the aid of electromagnetic coupling between the radiator and the parasitic element. This procedure was applied to other types of antenna designs [6, 7]. In principle, the parasitic element acts as a reactive loading for the improvement of the input impedance of the monopole antenna.

REFERENCES

1. S. Honda, M. Ito, H. Seki, and Y. Jinbo, A disc monopole antenna with 1:8 impedance bandwidth and omnidirectional radiation pattern, Proc ISAP'92, Sapporo, Japan, 1992, pp. 1145–1148.
2. N.P. Agrawal, G. Kumar, and K.P. Ray, Wide-band planar monopole antenna, IEEE Trans Antennas Propagat 46 (1998), 294–295.
3. M.J. Amman, Square planar monopole antenna, Proc IEE Nat Conf Antennas Propagat, York, England, 1999, pp. 37–40.
4. Z.N. Chen and Y.W.M. Chia, Impedance characteristics of trapezoidal planar monopole antennas, Electron Lett (submitted, Mar. 2000).
5. M. Hammoud, P. Poey, and F. Colombel, Matching the input impedance of a broadband disc monopole, Electron Lett 29 (1993), 406–407.
6. H. Nakano, M. Yamazaki, and J. Yamauchi, Electromagnetically coupled curl antenna, Electron Lett 33 (1997), 1003–1004.
7. K.M. Luk, C.L. Mak, Y.L. Chow, and K.F. Lee, Broadband microstrip antenna, Electron Lett 34 (1998), 1442–1443.

© 2000 John Wiley & Sons, Inc.

TWO-STAGE VANE LOADING OF GYRO-TWTs FOR HIGH GAINS AND BANDWIDTHS

Mukul Agrawal,¹ G. Singh,¹ P. K. Jain,¹ and B. N. Basu¹

¹Centre of Research in Microwave Tubes
Department of Electronics Engineering
Institute of Technology
Banaras Hindu University
Varanasi 221005, India

Received 18 April 2000

ABSTRACT: In this theoretical paper, we exploit the high-gain, through narrowband, potential of a vane-loaded gyro-TWT to suggest a two-section vane-loaded device configuration for large gains and bandwidths. We predict the lengths as well as the vane parameters and the background magnetic fields of the individual sections for the desired performance. © 2000 John Wiley & Sons, Inc. Microwave Opt Technol Lett 27: 210–213, 2000.

Key words: microwave tube; gyrotron, traveling-wave tube; high-power millimeter-wave amplifier

1. INTRODUCTION

Previous work [1] has reported the analysis of the effect of vane loading the cylindrical waveguide interaction structure of a gyro-TWT, an upcoming high-power millimeter-wave electron beam device based on the principle of cyclotron resonance maser instability, which has a potential application in high-resolution radar and high-information-density communication systems. Reasonably wideband gyro-TWTs have been realized by optimizing the beam and the background magnetic field parameters [1, 2]. However, bandwidths as wide as those obtainable in conventional TWTs cannot be attained in gyro-TWTs. This is due to a narrowband coales-

cence between the beam-mode line and the waveguide-mode hyperbola in the $\omega - \beta$ dispersion plot at the operating point near the cutoff frequency of the waveguide, where the group velocity increases rapidly [3].

One of the methods of widening the bandwidth of a gyro-TWT is to simultaneously taper both the cross section of the waveguide and the background magnetic field. The method gives large bandwidths, although at the cost of gain [4–6]. The low gain in this method is attributable to a small portion of the interaction length being effective for a narrow range of frequencies. Attempts were also made to widen the coalescence bandwidth. Modifying the dispersion characteristic of the waveguide by means of suitable loading can do this. For example, dielectric loading, in the form of a longitudinal dielectric rod placed at the axis of the waveguide or a dielectric lining on the inner wall of the waveguide, was suggested [7, 8]. However, the method has a difficulty arising from the charging of the dielectric, and associated heating, a problem that can be alleviated only by complicated schemes, like thin metal coating of the dielectric surface [7, 8]. Another method suggested to improve the coalescence bandwidth is to load the waveguide by axially periodic metal disks [9]. The loading of the waveguide by wedge-shaped metal vanes projecting radially inward from the waveguide wall, a method used for a low-voltage and low-magnetic-field operation for gyrotron sources [10, 11], has also been analyzed in the gyro-TWT (amplifier) configuration [1, 12, 13]. The azimuthally periodic vane loading, although it showed promise for high gains, unlike the axially periodic disk loading, cannot widen the coalescence bandwidth, and hence yield wide device bandwidths.

In the present paper, we propose a two-stage vane-loaded gyro-TWT, in which the interaction structure of the device consists of a vane-loaded cylindrical waveguide divided into two sections of dissimilar vane dimensions. The motivation is to exploit the high-gain potential of vane loading, and add the gain–frequency responses of the individual sections, each of which can be suitably controlled by the vane and the magnetic field parameters, for a wideband overall response of the two-section device at a high-gain value.

2. GAIN COMPUTATION

The small-signal dispersion relation of a small-orbit gyro-TWT in a smooth-wall cylindrical waveguide, excited in the transverse-electric (TE) mode, is available in the literature [14, 15]. In deriving the relation, the tenuous-beam approximation was made, large transverse electron velocities (v_t) were assumed, and operation was considered close to the s th beam-mode harmonic resonance, where the cyclotron resonance maser instability prevails over the Weibel instability [14, 15]. The dispersion relation of the gyro-TWT can be interpreted to write the conventional-TWT, Pierce-type gain equation [14, 15]:

$$G = A + BCN \quad (1)$$

where A and B are the launching loss and the growth rate parameters, respectively. A is expressible in terms of the three roots of $\delta = \delta_1, \delta_2, \delta_3$ of the cubic equation $\delta(\delta + jb)^2 = j$ (to which the gyro-TWT dispersion relation can be reduced). Here, b is a velocity synchronization parameter, which involves the beam, magnetic field, and waveguide parameters. Out of the three roots of δ one, say δ_1 , has a positive real part x_1 , say, which corresponds to a growing

wave. B is expressible in terms of x_1 . C is the Pierce gain parameter, defined as $C = (KI_0/4V_0)^{1/3}$, where V_0 and I_0 are the beam voltage and the beam current, respectively. K is an impedance parameter similar to the interaction impedance of a conventional TWT. K can be expressed as a function of the beam pitch factor α_0 , hollow beam radius r_H , Larmor radius r_L , waveguide wall radius r_W , and waveguide-mode axial phase propagation constant β and cutoff wavenumber k_c . N is the interaction length expressed in terms of the number of guide wavelengths $2\pi/\beta$ [14, 15].

To quickly estimate the effect of vane loading, one may use the gain expression (1), which was otherwise derived for the gyro-TWT in a smooth-wall cylindrical waveguide. In doing so, however, one has to take in this expression the appropriate values of β and k_c for the vane-loaded structure. The latter are obtainable from the solution of the cold (beam-absent) dispersion relation [1, 13], which is expressible in terms of the number of vanes N_V , the vane wedge angle ϕ_V , the radius of the inner vane edge r_V , and the waveguide wall radius r_W (Fig. 1).

3. RESULTS AND DISCUSSION

We have considered here two schemes for two-section vane loading a gyro-TWT. In one scheme, labeled as I, we have made the vane depths different, but have kept the same vane wedge angles in the two sections of the waveguide. In another scheme, labeled as II, the vane angles in the two sections have been made different, but the vane depths have been kept the same in the two sections. In general, the two sections have different lengths. For one of the sections, say, section 1, the magnetic field is slightly “detuned” from synchronism, so that the beam-mode dispersion line intersects the waveguide-mode dispersion curve at two different points. This results in a gain–frequency response of the section that shows two peaks corresponding, respectively, to the two crossing intersection points. Similarly, the background magnetic field for the second section, say, section 2, is adjusted so that it becomes “tuned” to the usual “grazing-intersection”-point flux density value B_g of the conventional gyro-TWT operation, such that only one peak is obtained in the gain–frequency response of this section, that falls around the trough between the two peaks of the gain–frequency response of the first section. The frequency at which the peak of the gain–frequency response of the second section occurs is controlled by adjusting the vane parameters of the second

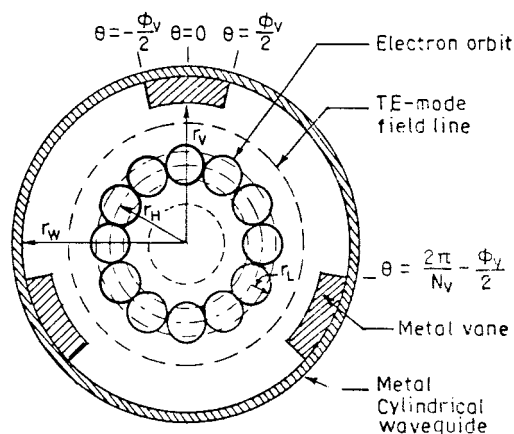


Figure 1 Structure cross section, typically showing three vanes

section. The gains of the individual sections can be controlled by their lengths.

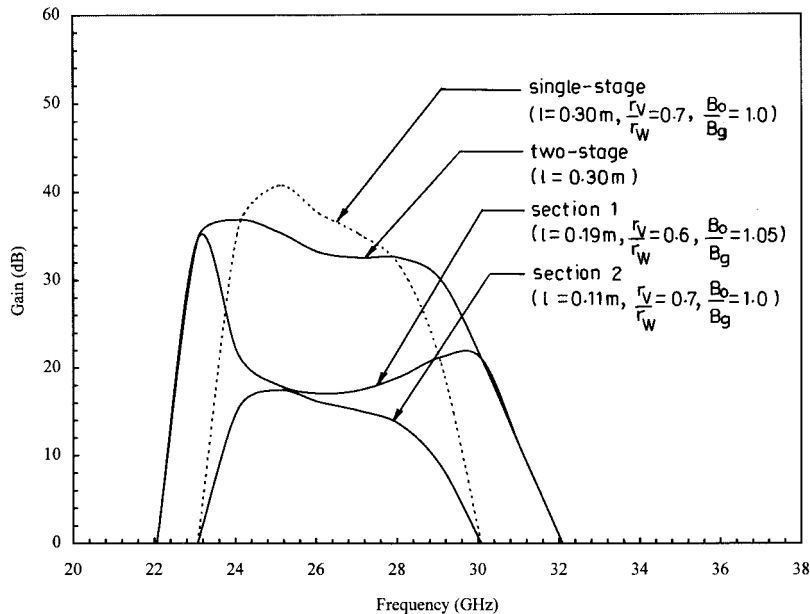
The gains of the individual sections 1 and 2 of the device, for both schemes I and II, have been computed with the help of (1). The gain–frequency response has shown two peaks for section 1 and one peak for section 2 that lies between the peaks of section 1 (Fig. 2). The gain of the two-stage device, obtained by adding the gain contributions from the individual sections, shows a wideband frequency response compared to a single-stage device of the length equal to the overall length of the two-section device, although at the cost of some gain value (Fig. 2). From the standpoint of matching between the two sections, certainly, scheme II, which has no radial discontinuity, enjoys a better potential than scheme I. It is also

evident that the two-stage vane-loaded gyro-TWT enjoys a larger gain than a distributed gyro-TWT in which the waveguide cross section and the background magnetic field are simultaneously tapered, such that only small different-length portions become effective at different frequency values.

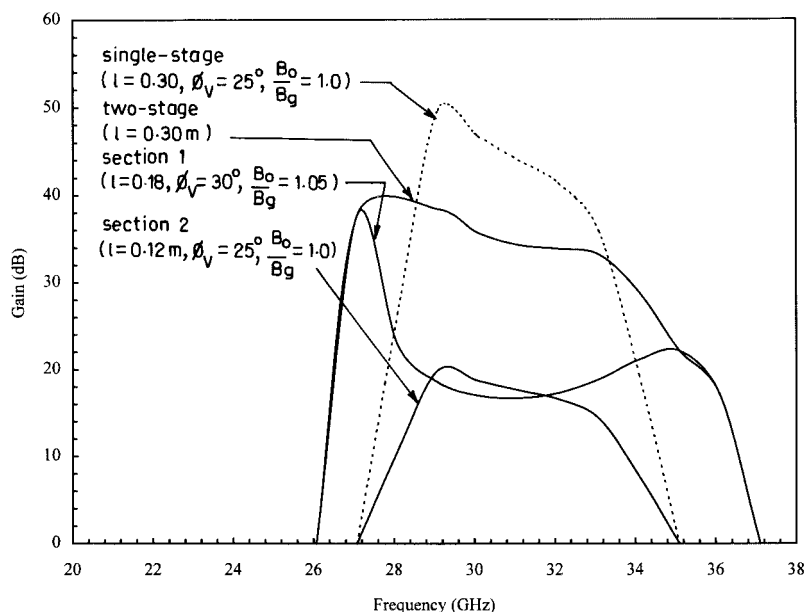
Thus, in this paper, by a simple theory, we have suggested a method for obtaining wideband, gyro-TWTs in an all-metal structure at high-gain values.

REFERENCES

1. G. Singh, P.V. Bhaskar, S.M.S. Ravi Chandra, P.K. Jain, and B.N. Basu, Control of the gain-frequency response of a vane-loaded gyro-TWT by beam and magnetic field parameters, *Microwave Opt Technol Lett* 24 (2000), 140–145.



(a)



(b)

Figure 2 Gain–frequency response of a two-stage vane-loaded gyro-TWT (a) in scheme I ($N_V = 4$, $\phi_V = 45^\circ$), and (b) in scheme II ($N_V = 4$, $r_V/r_W = 0.6$) for TE_{01} waveguide mode and fundamental beam-harmonic mode [$V_0 = 70$ kV, $I_0 = 9$ A, $\alpha_0 = 0.5$, $r_H/r_W = 0.58$, $r_L/r_V = 0.1$, $r_W = 5.9$ mm]

2. A.J. Sangster, Small signal bandwidth characteristics of a traveling-wave gyrotron amplifier, *Int J Electron* 51 (1981), 583–594.
3. Rekiouak and B.R. Cheo, Wide band gyrotron traveling wave amplifier analysis, tech rep POLY-WRTI-1531-88, Weber Res Inst, Polytechnic University, Farmingdale, NY, 1987.
4. K.R. Chu, Y.Y. Lau, L.R. Barnett, and V.L. Granatstein, Theory of a wide-band distributed gyrotron traveling-wave amplifier, *IEEE Trans Electron Devices* ED-28 (1981), 866–871.
5. G.S. Park, J.J. Choi, S.Y. Park, C.M. Armstrong, A.K. Ganguly, R.H. Kyser, and R.K. Parker, Gain broadening of two stage gyrotron travelling wave tube amplifier, *Phys Rev Lett* 74 (1995), 2399–2402.
6. A.K. Ganguly and S. Ahn, Large signal theory of two-stage wideband gyro-TWT, *IEEE Trans Electron Devices* ED-31 (1984), 474–480.
7. K.C. Leou, D.B. McDermott, and N.C. Luhmann, Jr., Dielectric-loaded wideband gyro-TWT, *IEEE Trans Plasma Sci* 20 (1992), 188–196.
8. S.J. Rao, P.K. Jain, and B.N. Basu, Two stage dielectric loading for broadbanding a gyro-TWT, *IEEE Electron Device Lett* 17 (1996), 303–305.
9. J.Y. Choe and H.S. Uhm, Theory of gyrotron amplifiers in disc or helix loaded waveguides, *Int J Electron* 53 (1982), 729–741.
10. Y.Y. Lau and L.R. Bennett, Theory of low magnetic field gyrotron (gyromagnetron), *Int J Infrared Millimeter Waves* 3 (1982), 619–643.
11. K.R. Chu and D. Dialetis, Kinetic theory of harmonic gyrotron oscillator with slotted resonance structure, *Infrared Millimeter Waves* 13 (1985), 45–75.
12. C.K. Chong, D.B. McDermott, A.J. Balkcum, and N.C. Luhmann, Jr., Nonlinear analysis of high-harmonic slotted gyro-TWT amplifier, *IEEE Trans Plasma Sci* 20 (1992), 176–187.
13. G. Singh, S.M.S. Ravi Chandra, P.V. Bhaskar, P.K. Jain, and B.N. Basu, Analysis of an azimuthally-periodic vane-loaded cylindrical waveguide for a gyro-travelling-wave tube, *Int J Electron* 86 (1999), 1463–1479.
14. B.N. Basu, *Electromagnetic theory and applications in beam-wave electronics*, World Scientific, Singapore, 1996.
15. A.J. Sangster, Small-signal analysis of the travelling-wave gyrotron using Pierce parameters, *Proc Inst Elect Eng* 127 (1980), 45–52.

© 2000 John Wiley & Sons, Inc.

ON THE USE OF THE MATRIX-PENCIL TECHNIQUE TO IMPROVE THE COMPUTATIONAL EFFICIENCY OF THE FDTD METHOD

Feng Cheng¹ and Quanrang Yang¹

¹State Key Laboratory of Millimeter Waves
Southeast University
Nanjing 210096, P.R. China

Received 3 April 2000

ABSTRACT: In this paper, we apply the matrix-pencil (MP) technique to extract the complex exponentials from a truncated time response computed by using the FDTD method. To obtain accurate parameters without further FDTD computations, the truncated time response is efficiently extended into the future by summing the complex exponentials with complex coefficients. Three examples are analyzed to illustrate the efficiency of the matrix-pencil method. © 2000 John Wiley & Sons, Inc. *Microwave Opt Technol Lett* 27: 213–216, 2000.

Key words: matrix pencil; FDTD; interpolation and extrapolation

I. INTRODUCTION

In previous work [1–3], it has been demonstrated that an FDTD time record long enough for accurate parameter estimation can be efficiently obtained from a relatively short time record by using an extrapolation scheme based on the Prony method, AR model, and system identification techniques. But the main problems with these methods are the difficulty involved in determining the order of the model, and their sensitivity to noise in the data.

The application of an alternative scheme based upon pencil-of-function techniques [4–6], called the matrix pencil (MP), is discussed in this paper. This technique is formed by fitting the early FDTD response to an exponential model. The remaining part of the time response is efficiently extended by summing the complex exponentials whose complex coefficients are obtained from singular-value decomposition (SVD) and the least squares problem (LSP). This approach confers robustness to the MP technique, and provides a simple and effective criterion for the selection of the order of the model. To illustrate the efficiency of this technique, we have considered three examples: the resonant frequency of the dominant mode of a microstrip resonator [7], and the *S*-parameters and heat conduction [8] of a type of MMIC package.

II. MATRIX-PENCIL TECHNIQUE

The FDTD time response can be approximated as a sum of damped complex exponentials:

$$y_k = x_k + n_k = \sum_{i=1}^M r_i z_i^k + n_k \quad (1)$$

where $k = 0, 1, \dots, N-1$ is the time index, $z_i = \exp(s_i) = \exp(\alpha_i + j\omega_i)$ are the poles, n_k indicates additional noise, and y_k denotes the observed FDTD sequence of length N . The model parameters r_i , ω_i , and α_i represent the complex amplitudes or residuals, angular frequencies, and damping factors, respectively. It is clear that r_i and s_i should, respectively, be in complex conjugate pairs for a real-valued y_k .

Following the idea of the pencil-of-function method [4–6], we define the matrices Y_1 and Y_2 as

$$Y_1 = [\vec{y}_0, \vec{y}_1, \dots, \vec{y}_{L-1}] \quad (2)$$

$$Y_2 = [\vec{y}_1, \vec{y}_2, \dots, \vec{y}_L] \quad (3)$$

where $\vec{y}_i = [y_i, y_{i+1}, \dots, y_{i+N-L-1}]^T$ and $M \leq L \leq N - M$.

We form a matrix pencil $Y_2 - \lambda Y_1$, where λ_i are the generalized eigenvalues of Y_2 and Y_1 . The generalized eigenvectors \mathbf{q}_i satisfy

$$Y_2 \vec{q}_i = \lambda_i Y_1 \vec{q}_i. \quad (4)$$

Using singular-value decomposition (SVD), Y_1 can be expressed as [9]

$$Y_1 = UDV^H \quad (5)$$

where U , V are unitary matrices of left and right singular vectors, respectively. D is a diagonal matrix of singular values, and H means conjugate transpose. The generalized